Ferromagnetism and local electronic properties of rutile $Ti_{1-x}Fe_xO_2$ single crystals

L. Sangaletti,[1] M. C. Mozzati,[2] G. Drera,[1] P. Galinetto,[2] C. B. Azzoni,[2] A. Speghini,[3] and M. Bettinelli[3]
[1]*Dipartimento di Matematica e Fisica, Università Cattolica, Via dei Musei 41, 25121 Brescia, Italy*
[2]*CNISM and Dipartimento di Fisica "A. Volta" Università di Pavia, Via Bassi 6, 27100 Pavia, Italy*
[3]*Dipartimento Scientifico e Tecnologico, Università di Verona, Strada Le Grazie 15, 37134 Verona, Italy*
(Received 13 February 2008; revised manuscript received 4 June 2008; published 28 August 2008)

An experimental evidence of the effects of iron on the magnetic and local electronic properties of TiO_2 single crystals is provided. When ferromagnetic rutile TiO_2 single crystals are doped with Fe ions, an enhancement of the saturation magnetic moment is observed, along with a transfer of electrons to Fe 3*d* and Ti 3*d* levels. Indeed, the analysis of core-level photoemission data shows that addition of iron has the effect (i) to promote electron charge transfer from O 2*p* band to localized Fe 3*d* orbitals and (ii) to reduce titanium ions by introducing $3d^1$ electronic states in the otherwise empty 3*d* band of pure TiO_2. These effects, resulting from the incorporation of both transition-metal ion dopants and oxygen vacancies, increase the local magnetic moments that can contribute to long-range ferromagnetic ordering.

DOI: 10.1103/PhysRevB.78.075210 PACS number(s): 75.50.Pp, 73.20.At, 79.60.−i, 81.10.Fq

I. INTRODUCTION

The magnetic properties of doped rutile TiO_2 still represent a challenge both from a theoretical and experimental point of view.[1] While evidences of intrinsic ferromagnetism (FM) in these systems has been provided by several research groups, the mechanism underlying the coupling between magnetic moments and the onset of ferromagnetism are still under debate. There is an emerging evidence that FM in these systems is a complex phenomenon, which involves the interplay between oxygen vacancies, doping impurities, and their effects on the density and localization of charge carries. The preparation of suitable samples has been mainly achieved by producing thin films with pulsed laser deposition, reactive sputtering, molecular-beam epitaxy, and ion implantation.[2] Depending on the thin-film growth conditions, their structural, magnetic, and transport properties[3,4] may present different behaviors also for nominally identical stoichiometries and doping levels. Only recently the growth of pure and transition metal (TM) doped TiO_2 rutile single crystals, which display FM at room temperature (RT), has been reported.[5] This kind of growth is carried out in near equilibrium conditions by a final cooling of the melt, which may take several days. These conditions are quite different from the out of equilibrium conditions typical of laser ablation or RF sputtering and may offer a possible alternative route to produce homogeneous and segregation-free samples.

Furthermore, recent evidences of RT FM in undoped TiO_2 samples[5,6] have posed further questions about the role of 3*d* element doping in these oxides. The open problem is whether doping introduces FM or it just enhances the magnetism already present in the oxide host. Indeed, the mechanisms responsible for ferromagnetism in diluted magnetic oxides (DMO) are still under debate. According to a phase diagram recently proposed by Coey *et al.*,[7] ferromagnetism in these insulating oxides should arise from magnetic polarons above the percolation threshold.[8] In *n*-doped systems, these polarons localize around an oxygen vacancy, may polarize the magnetic moment of TM ions present in doped crystals and in thin films, and finally polarons may percolate to yield magnetic ordering. Mean-field theories (MFT) have also been considered,[8] being static MFT the most appropriate mean-field approach for strongly insulating DMO. As a general rule, for the onset of ferromagnetism it seems important to introduce defects in the lattice that yield, e.g., donor levels in *n*-doped oxides. Defects can already appear in the pure TiO_2 lattice but they can be increased by doping the lattice with nontetravalent TM ions. Furthermore, hybridization and charge transfer (CT) from oxygen 2*p* band to nominally empty *d* states of TiO_2 or to partially occupied 3*d* states of TM dopant are expected to play an important role to enhance the Curie temperature.

While ferromagnetism develops as a long-range order, the mechanisms underlying the magnetic coupling have to be searched on a more local scale, i.e., within the length scale of a few unit cells, as was recently proposed in theoretical studies based on *ab initio* electronic structure calculations.[9] Photoemission spectra of open shell TM impurities are known to be significantly influenced by intra-atomic multiplet splitting and also by interatomic CT effects, which in most cases involve a cluster of atoms composed of the TM atom and the nearest-neighbor ligand anions.[10] Therefore most of the analysis of core-level x-ray photoemission spectroscopy (XPS) spectra of open shell 3*d* TM oxides is carried out on a local scale represented by a (distorted) TMO_6 octahedral cluster, being the octahedral coordination of TM cations with oxygen anions quite often found in transition-metal monoxides and dioxides (e.g., MnO, FeO, CoO, NiO, and TiO_2). In this context, information on CT effects can be gained in the frame of configuration interaction (CI) impurity cluster model analysis of the experimental spectra, as recently proposed for Co-doped rutile TiO_2 thin films.[11] Likewise, the ionization state of the TM or Ti ions can be properly discussed upon an analysis of the core-level photoemission spectra.

The aim of the present study is to investigate and discuss the effects of iron doping on the magnetic and local electronic properties of FM rutile TiO_2 single crystals. While magnetization measurements show an enhancement of saturation magnetic moment when pure TiO_2 single crystals are doped with Fe ions, the analysis of core-level photoemission

data show that Fe doping promotes a CT from oxygen $2p$ band to the localized $3d$ levels of Fe. Furthermore, a reduction of titanium is observed, which adds electrons to the nominally empty Ti $3d$ band of stoichiometric rutile TiO_2.

II. EXPERIMENT

The growth of pure and doped single crystals was based on the dissolution of the titanium dioxide TiO_2 in molten $Na_2B_4O_7$ at high temperature, with spontaneous nucleation and crystal growth of TiO_2 achieved by the slow cooling (2 °C/hour) of the solution from 1100 to 750 °C. In the present case, iron concentration was nominally 5% atomic with respect to titanium although the actual concentration in the obtained crystals is below 1%. The crystals grew in the form of transparent needles elongated in the direction of the crystallographic c axis and their size were approximately $0.10 \times 0.05 \times 5.00$ mm^3. The sample crystallinity and phase was checked by x-ray diffraction and Raman spectroscopy. All crystals were found to be in the rutile phase. The iron content was evaluated by laser ablation inductively coupled plasma mass spectrometry (LA-ICP-MS), exploring the samples to a depth of about 50 μm. The iron content was estimated to be about 1 mol %, in agreement with previous results obtained with x-ray fluorescence probe. Typical needlelike crystals of iron-doped TiO_2, hereafter denoted as Fe:TiO_2, are shown in the inset of Fig. 1(a).

Static molar magnetization (M_{mol}) was measured at 2000 Oe from 362 to 2 K with a superconducting quantum interference device (SQUID) quantum design magnetometer. M_{mol} loops were collected at RT for magnetic fields (H) ranging between 0 and ± 4000 Oe.

Photoemission data were measured by using an Al-k_α source and a modified VG MkII spectrometer equipped with a 32 channel multichannel plate detector. X-ray photoemission spectra were collected at a base pressure of 2×10^{10} mbar with an energy resolution of 800 meV.

Micro-Raman spectra were collected at room temperature with a Dilor Labram spectrograph with a HeNe laser (632.8 nm) as an exciting source and a light power less than 10 mW at the sample.

III. RESULTS AND DISCUSSIONS

A. Magnetic measurements

M_{mol} vs H curves collected at RT with the external field H applied parallel to the crystal axis had shown a behavior seen as a superposition between a paramagnetic contribution and a weak hysteresis cycle [Fig. 1(a)]. The hysteresis loops, extracted from the experimental data after subtraction of the linear paramagnetic contribution, indicates that a ferromagnetic ordering, although weak, is already present at RT.[5] The dominant paramagnetic character for both samples is clearly evidenced in Fig. 1(b)—where the molar magnetic susceptibility (χ_{mol}), as obtained for the two samples by applying a 2000 Oe magnetic field parallel to the crystals c axis, is reported. Due to the low signal from the undoped sample with respect to the Fe:TiO_2 crystal, the curve for the undoped crystal is also shown in the inset with an expanded

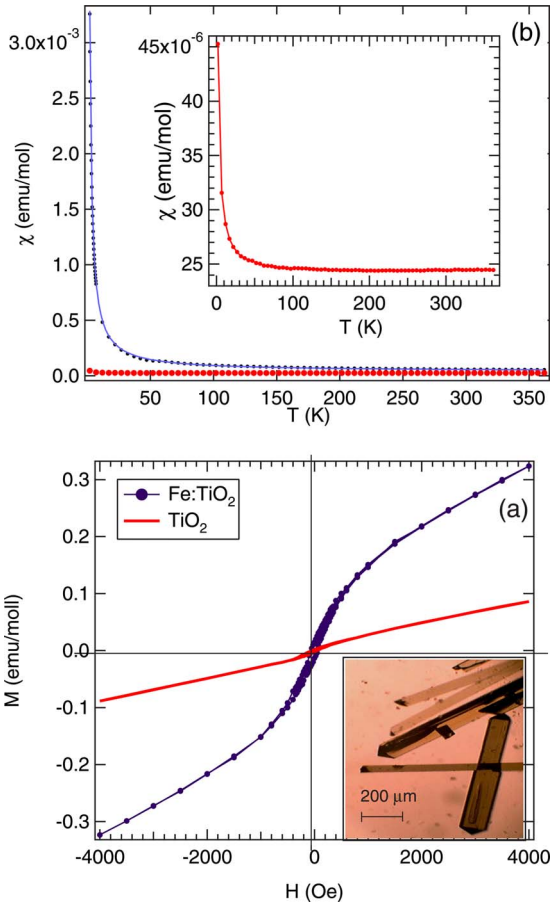

FIG. 1. (Color online) (a) Hysteresis loop measured on the Fe:TiO_2 and on the undoped TiO_2 crystals. The core electron diamagnetic contribution, as well as that of sample holder, has been subtracted from both cycles. The inset shows typical needlelike Fe:TiO_2 single crystals. (b) χ_{mol} vs T behavior for the Fe:TiO_2 and pure TiO_2 crystals. The inset shows the χ_{mol} curve for the undoped crystal drawn on an enlarged scale.

vertical scale. Even though no criticality is evident when the magnetization is plotted as a function of temperature, thus supporting the overall paramagnetic behavior, we stress that the data follow a modified Curie-Weiss law—i.e., $\chi = C/(T + \theta) + \chi_0$, with θ values roughly close to zero—when a 2000 Oe field is applied. A strictly constant additive value (χ_0) can be considered, consistently with the presence of a saturated magnetic phase. This can be regarded as the signature of ferromagnetic ordering, further confirmed by deviation from the linear behavior of the $1/\chi_{mol}$ curve. We point out that the observed strongly concave M_{mol} vs T curves is often a characteristic of insulating diluted magnetic semiconductor (DMS) systems (see, e.g., Ref. 8 and references therein).

By separately analyzing the paramagnetic and ferromagnetic contributions and by considering the most probable oxidation states for the Fe ions that is Fe^{3+} (spin 5/2), the resulting concentration of paramagnetic Fe ions results to be 0.22%. If we assume that iron ions are in Fe^{2+} oxidation state, the spin on iron sites is reduced to $S=2$ and the estimated concentration increases by a factor about 1.5. These values have been obtained by taking into account the contri-

bution of the undoped TiO_2 crystals that already contribute with a concentration of 1.47% paramagnetic ions (here a spin 1/2 is assumed for each ion). Paramagnetic ions in pure undoped TiO_2 can be related to oxygen vacancies that reduce Ti^{4+} ions to Ti^{3+}. From the hysteresis loops the molar saturation magnetization M_{Smol} can be deduced so that the contribution due to the addition of the TM ions to M_{Smol} results to be about 0.11 emu/mole for Fe. From these data the concentration of the ferromagnetic centers can be estimated by assuming again Fe^{3+} and a parallel spin alignment in the host matrix; the lower limit for the magnetic ions contributing to the ferromagnetic ordering at RT results to be only about 0.1%–0.2% of the TM paramagnetic centers. Therefore, the data presented above showed that (i) ferromagnetism is already present in undoped crystals, in agreement with recent findings,[6] and the addition of Fe impurities enhances the magnetic behavior; (ii) the ions that contribute to ferromagnetic order at RT are only a fraction of the paramagnetic ions, which may have implications for magnetic polaron percolation models,[8] where it was predicted that the fraction of volume taken from the infinite percolation cluster that yields ferromagnetism is still low at RT.

B. Photoemission measurements

The effect of iron impurities on the electronic properties of the doped sample is discussed by examining the Fe $2p$ core-level XPS spectra of the Fe:TiO_2, FeO, and Fe_2O_3 single crystals, along with the calculated spectra of the Fe $2p$ core line with a CI impurity cluster model. Figure 2(a) shows the Fe $2p$ XPS spectrum obtained from Fe:TiO_2 single crystals. This spectrum is compared with those collected from FeO single crystals[12] [Fig. 2(b)] and with those recently reported for Fe_2O_3 single crystals[13] [Fig. 2(c)]. As can be observed, these spectra show several differences. The basic spectrum consists of a spin-orbit split doublet with a binding energy (BE) of 710 (A) and 723 eV (C). Additional satellite structures (B and D) are found at higher BEs with respect to each doublet component. The spectral weight identified by B and D structures may change in different compounds. Indeed, it looks lower in Fe_2O_3 and larger in FeO and Fe:TiO_2, and the binding energy of both B and D satellites decreases from Fe_2O_3 to Fe:TiO_2. Moreover, the Fe $2p$ XPS spectrum of the nominally trivalent iron of Fe_2O_3 is very similar to the corresponding spectrum in $LiFeO_2$,[14] indicating that for trivalent iron ions the satellite spectral weight is much lower and is found at higher BEs with respect to the formally divalent ions. Finally, the Fe $2p$ XPS spectrum Fe:TiO_2 also shows one additional weak feature (B_1) at BE=717 eV. This feature has a counterpart in the region of satellite D, which appears larger than the corresponding structure in FeO and Fe_2O_3.

In order to provide a better identification of the spectral weight found on the high BE side of each of the spin-orbit split lines, a fit of the Fe $2p$ XPS core line of Fe:TiO_2 has been carried out by using a curve defined as the sum of six Gaussian peaks. The peaks have been labeled consistently with the labels introduced to identify the main experimental structures. The first three peaks are labeled as A, B, and B_1

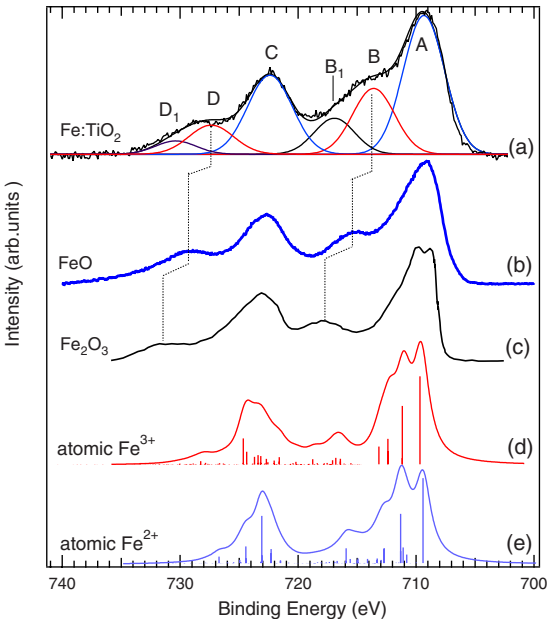

FIG. 2. (Color online) Fe $2p$ XPS spectrum from the Fe:TiO_2 single crystal (a). The spectrum has been fit with a set of Gaussian curves in order to single out the main peaks contributing to the total spectral weight. The Gaussian curves are labeled A, B, B_1, C, D, and D_1. The sum of this contribution yields the total fitting curve represented with a thick solid line. This spectrum is compared with those collected from (b) FeO (Ref. 12) and (c) Fe_2O_3 single crystals (Ref. 13). Calculated Fe $2p$ photoemission spectrum for (d) Fe^{3+} and (e) Fe^{2+} ions in the atomic limit.

and are used to fit the Fe $2p_{3/2}$ contribution, whereas the second set of peaks (C, D, and D_1) is used to fit the Fe $2p_{1/2}$ contribution. For the fitting procedure several constraints have been used. As first, the intensity ratio between the sum of A, B, and B_1 peaks and the sum of C, D, and D_1 peaks has been set to two, in agreement with the degeneracy of the spin-orbit split electronic states. Furthermore, the linewidth was maintained in a narrow range of values (HWHM $\simeq$2.0–2.2 eV), where HWHM stands for half-width at half maximum, to avoid unphysically broad Gaussian peaks. As can be observed from the fitting results, the B_1 and also the D_1 features bring a significant contribution to the spectral weight. Attempts to use only four Gaussian curves failed to fit the experimental curve mainly because the spectral weight in the 715–720 eV BE range results to be underestimated unless one resorts to introduce a quite broad Gaussian curve in the region of peak B to compensate for the lack of the third (B_1) peak. The energy separation between the six Gaussian centroids, as well as the intensity ratio between the Gaussian areas obtained from the best fitting to the experimental data, have been used as a reference for the impurity cluster calculations (see below).

In Figs. 2(d) and 2(e) the calculated Fe $2p$ photoemission spectra are shown. These calculations are based on intra-atomic interactions alone for isolated Fe^{2+} and Fe^{3+} ions.[15] All the calculated features are ascribed to multiplet effects arising from the $2p^53d^5$ or $2p^53d^6$ final-state configurations of the Fe^{3+} and Fe^{2+} ions, respectively. As can be observed, the spectral weight in the BE region where satellite features

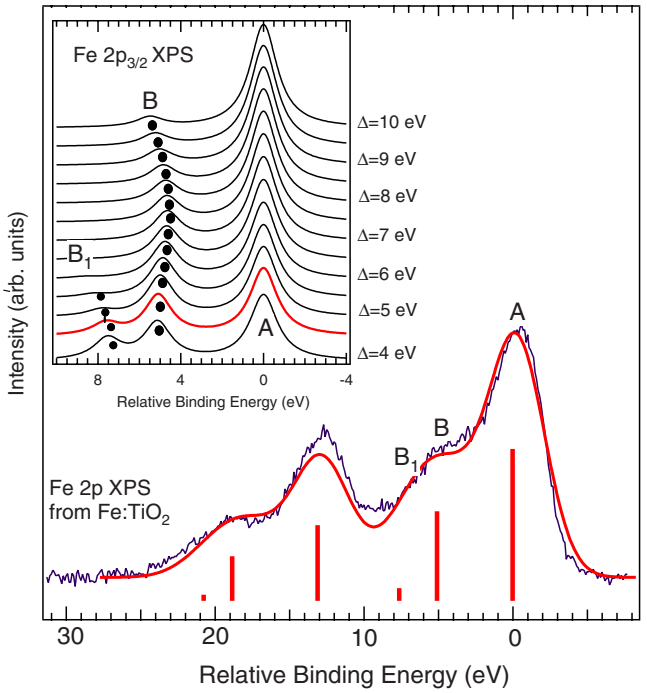

FIG. 3. (Color online) Calculated Fe^{2+} XPS spectrum for $\Delta=4.5$ eV, $T=2.49$ eV, $Q=6.8$ eV, and $U=5.7$ eV (thick line). The calculated spectrum is compared with the experimental data of the $Fe:TiO_2$ single crystal. The energy and length of the vertical bars represent the eigenvalues and intensities calculated with the parametrized CI cluster model. Inset: Calculated Fe^{2+} $2p_{3/2}$ XPS spectra for CT energies ranging from $\Delta=4.0$ to 10 eV, with 0.5 eV steps. The other model parameters used in the calculation are: $T=2.49$ eV, $Q=6.7$ eV, and $U=5.4$ eV.

are expected is much lower than that observed in the experimental data. The increase in the spectral weight from the atomic to the solid-state environment for the Fe ions is usually ascribed to CT effects from O $2p$ to TM $3d$ partially empty states (see, e.g., Ref. 16 for the case of Ni dihalides). Mostly atomic behavior is a characteristic of systems with a high CT energy, such as MnO,[17] and departure from atomic behavior occurs when the CT energy decreases, allowing for CT from the ligand (here O $2p$) orbitals to localized transition-metal $3d$ levels. In order to evaluate the extent of CT effects in our system, a simple analysis of the Fe $2p$ XPS spectra was carried out on the basis of CT effects alone. By assuming a configuration interaction scheme, we can estimate the effect of CT on the spectral weight of a core line, e.g., the A peak in the spin-orbit split doublet, as shown in the inset of Fig. 3, where the Fe $2p_{(3/2)}$ spectral weight has been calculated for different CT energies (Δ).

In the configuration interaction approach several configurations, denoted as d^n and $d^{n+1}\underline{L}$ ($\underline{L}$ denotes a ligand hole), are used to describe the open shell of the $3d$ transition-metal ion during the photoemission process. Accordingly, the initial state wave function is written as

$$\Psi_{GS} = a_1|d^n\rangle + a_2|d^{n+1}\underline{L}\rangle + a_3|d^{n+2}\underline{L}^2\rangle, \qquad (1)$$

where $\underline{L}$ denotes a configuration with a p hole in the anion states. In the present case, the p hole represents the CT from the O $2p$ levels to Fe $3d$ levels. The CT energy is defined as $\Delta=E(d^{n+1}\underline{L})-E(d^n)$, whereas the Coulomb d-d interaction is represented by $U=E(d^{n-1})+E(d^{n+1})-2E(d^n)$ [where $E(d^n\underline{L}^m)$ is the center of mass of the $d^n\underline{L}^m$ multiplet]. The Coulomb and CT energies are usually regarded as model parameters. Interaction between $d^{n+m}L^m$ and $d^{n+m+1}\underline{L}^{m+1}$ configurations is accounted for by the T_{pd} off-diagonal term in the Hamiltonian matrix.

In the case of core-level photoemission the final-state interaction between the core hole and the $3d$ electrons in the outer shell is explicitly accounted for by an energy parameter Q. Therefore the CT term is corrected as Δ-Q upon creation of the core hole. The final-state wave function is given by $\Psi_{i,fs}=c_{i,1}|\underline{c}d^n\rangle+c_{i,2}|\underline{c}d^{n+1}\underline{L}\rangle+\ldots$, where $\underline{c}$ represents the core hole. The spectral weight in a photoemission experiment is calculated—in the sudden approximation—by projecting the final-state configurations on the ground state, i.e., $I_{XPS}(BE) \propto \Sigma_i|\langle\Psi_{GS}|\Psi_{i,fs}\rangle|^2\delta(BE-\varepsilon_i)$, where $|\langle\Psi_{GS}|\Psi_{i,fs}\rangle|^2=|a_1c_{1,i}+a_2c_{2,i}+\ldots|^2$ and the sum is run over all final-state configurations $|\Psi_{i,fs}\rangle$ with energy ε_i.

From the results shown in the inset of Fig. 3, as first we observe that CT effects increases when the energy Δ of the CT parameter decreases from 10 eV down to 4 eV, high CT energies representing strongly ionic Fe-O bonds. As the CT energy decreases, the weight of satellite B increases and its energy moves to lower BE. Finally, a further structure (B_1) appears for low CT energies (below about 5 eV). This seems to be the case of the Fe core-level data of $Fe:TiO_2$, where also a weak satellite, B_1, appears at about BE=717 eV.

In Fig. 3 the Fe^{2+} XPS spectrum calculated with $\Delta=4.5$ eV, $T=2.49$ eV, $Q=6.7$ eV, and $U=5.4$ eV is shown (thick line), which displays a good agreement with the experimental data (thin line). Moreover, these parameter values well matches those reported in the literature for iron oxides.[18] For the present parametrized impurity cluster calculations, the energy separation between the six Gaussian peaks, as well as the intensity ratio between the Gaussian areas, obtained from the best fitting to the experimental data [Fig. 2(a)] have been used as a reference. Indeed, the parameter set yielding the theoretical spectrum was obtained by looking for the calculated spectral weight, which best matched the intensity ratio and relative energy of the A, B, and B_1 peak values resulting from the fitting presented in Fig. 2(a). For the parameter values an error bar can also be provided, which is ±0.5 eV for Δ, Q, and U, and ±0.25 eV for T. Attempts to reproduce the experimental data by using higher Δ values failed because the third (B_1) peak intensity resulted virtually quenched already for $\Delta=6$ eV. In turn, Δ values below 4 eV yielded a very large intensity for the B structure with respect to the main line A. The inset of Fig. 3 shows the calculated Fe $2p_{3/2}$ spectra for a wide range of Δ values (from 4 to 10 eV). Here, the calculated intensities have been convoluted with a narrow Lorentzian curve in order to clearly show change of spectral weights and binding energies with Δ.

On the basis of the comparison between spectra with different iron valence, as well as by considering the effects of CT on the energy and intensity of satellite features, we ascribe the Fe $2p$ spectral features observed in $Fe:TiO_2$ to Fe^{2+} ions. From the point of view of iron cations, the system

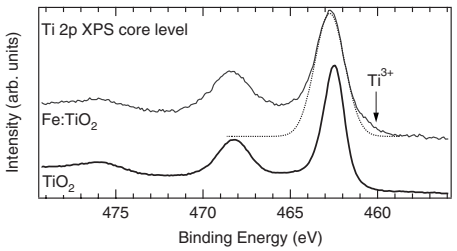

FIG. 4. Ti $2p$ XPS spectrum from the Fe:TiO_2 single crystal (thin line). This spectrum is compared with that collected from a stoichiometric TiO_2 110 single-crystal surface (thick line). The vertical arrow indicates the contribution of Ti^{3+} ions. A symmetric Gaussian peak has been drawn below the Ti $2p_{3/2}$ core line of Fe:TiO_2 in order to point out the asymmetry of this peak on the low BE side.

behaves as a strongly correlated system—displaying both d-d on-site correlations and CT correlations, which are a prerequisite for charge-carrier localization underlying the magnetic polaron model for strongly insulating oxides.[7,8]

In the high spin configuration, the Fe^{2+} oxidation state indicates that a $t_{2g}^4 e_g^2$ configuration should be assumed for Fe^{2+} in an octahedral crystal field. This level occupancy favors the interaction between Fe impurities and the nearest-neighbor Ti cations, as already observed for high spin Co^{2+} ions in rutile.[11] In fact, the high spin Fe^{2+} state has partially unoccupied t_{2g} orbitals that are expected to significantly hybridize with the Ti $3d$ t_{2g} orbitals enabling a direct t_{2g}-t_{2g} hybridization along the edge sharing MO_6 octahedra (M=Ti or Fe).

Finally, according to Eq. (1), the number of $3d$ electrons in the ground state, $\langle n_{3d} \rangle$, of the TM ion is given by

$$\langle n_{3d} \rangle = n \cdot |a_1|^2 + (n+1) \cdot |a_2|^2 + \ldots \quad (2)$$

and the increase of this number with respect to the nominal number of $3d$ electrons n (e.g., $n=6$ for Fe^{2+} ions) indicates the extent of CT. Here the sum is carried out on the number of configurations used to describe the ground state. With a Δ value of 4.5 eV, $\langle n_{3d} \rangle$ is estimated to be about 6.19, i.e., the density of $3d$ electrons on the Fe cation site has increased by about 30%, and that of $2p$ electrons delocalized on the six nearest-neighbor oxygen anions has decreased by about 30%.

This evidence supports the hypothesis that in TM-doped TiO_2 crystals with ferromagnetism enhanced by the addition of magnetic impurities to the host lattice, CT effects from the host lattice to the TM cation may contribute to enhance the hole density around TM impurities. This mechanism adds to the holes already created in the host lattice by replacing Ti^{4+} ions with nominally Fe^{2+} ions.

On the other hand, we observed that oxygen vacancies are expected to have implications on ionization state of Ti cations. Indeed, Ti^{3+} ions were found to contribute to the Ti $2p$ spectral weight of the present samples as a small shoulder on the low BE side of Ti $2p_{3/2}$ core line, as marked in Fig. 4 with a vertical arrow. This effect is well known when oxygen vacancies are introduced in TiO_2 single crystals by, e.g., ion bombardment in ultra-high-vacuum conditions.[19] A reduction of Ti ions is observed along with the oxygen substoichiometry induced by sputtering. Likewise, in TM-TiO_2 interfaces, the evaporation of Fe on TiO_2 single crystals is known to yield a Ti reduction,[19] i.e., an increase of the Ti $3d$ electron count with respect to $3d^0$. Furthermore, the width of the Ti $2p$ XPS core line of the Fe:TiO_2 crystal is larger than the corresponding line collected from the 110 surface of a pure rutile TiO_2 single crystal. This evidence may indicate that the addition of Fe ions introduces lattice disorder, which affects the electron potential around titanium ions and ultimately results in a broadening of the Ti $2p$ XPS core lines, as already observed in metal alloys.[20]

TABLE I. Linewidth Γ and frequency ω of the E_g and A_g Raman bands of Fe-doped and undoped rutile TiO_2.

Crystal	Γ_{E_g} (cm^{-1})	ω_{E_g} (cm^{-1})	Γ_{A_g} (cm^{-1})	ω_{A_g} (cm^{-1})
Fe:TiO_2	42.82	442.47	39.96	609.23
TiO_2	41.16	442.46	38.78	609.30

To support this thesis, we have also analyzed the linewidth of the Raman bands collected from the undoped and Fe-doped crystals. The detailed evaluation of the Raman parameters (i.e., linewidth, Γ, and peak position, ω) has been performed by a best fitting procedure using Lorentzian curves and the best fit values are reported in Table I for the two main Raman modes of rutile structure for both the Fe-doped and the pure TiO_2 crystals. We note that the peak energies are insensitive to the dopant, as expected. For the linewidth a weak increase is observed in the Fe-doped with respect to pure compound. This fact can be due to an increased disorder in doped crystal, which in turn could be connected to the increase of anionic vacancies.

This finding is consistent with what we have observed for the Ti $2p$ XPS core lines, and it also shows that the disorder induced broadening of the lines is a bulk effect. In fact, the scattered photons in the Raman experiment are collected from the bulk of the crystal and not from the topmost surface layers, as is the case of the photoemission probe.

IV. CONCLUSIONS

In summary, we have provided an experimental evidence of the effects of iron on the magnetic and local electronic properties of pure TiO_2 single crystals. These effects are (i) an enhancement of ferromagnetic behavior when pure TiO_2 single crystals are doped with Fe ions; (ii) a CT form O $2p$ band to localized Fe $3d$ energy levels, which adds to aliovalent substitution of Fe^{2+} for Ti^{4+} as a mechanism to enhance the hole density in these ferromagnetic crystals; and (iii) titanium reduction to Ti^{3+} ions and local disorder around these ions.

These results indicate that iron impurities are able to trigger mechanisms that yield an electron transfer both to the partially occupied Fe $3d$ states and to the otherwise empty Ti $3d$ levels. It is worth observing that electrons in $3d$ bands are usually regarded as strongly correlated, both in the case

of Mott-Hubbard and charge transfer insulators.[21] In fact, hopping mechanism leading to conduction are, e.g., hindered by the Mott-Hubbard U correlation energy if this energy is larger than $w/2$, where w is the $3d$ electron bandwidth. Likewise, hopping mechanisms are hindered by the CT energy if Δ is larger than $W/2$, where W is the bandwidth of the O $2p$ electronic states. According to the phase diagram drawn in Refs. 7 and 22 for n-doped DMO, the present $Fe:TiO_2$ compound should be a ferromagnetic metal if we assume the density of iron cations and oxygen vacancies estimated from the magnetization data. In turn, our $Fe:TiO_2$ single crystals are strong insulators, which indicates that electron-electron correlations are at work and may shift the border between FM-insulator and FM-metal regions in the phase diagram to larger values of the density of oxygen vacancies.

ACKNOWLEDGMENTS

We are all greatly indebted to C. B. Azzoni who has recently passed away. He strongly encouraged and supported these investigations and significantly contributed to the analysis and interpretation of the present experimental results. G.D. acknowledges the financial support from the Cariplo Foundation.

[1] For a recent review, see, e.g., J. M. D. Coey, Curr. Opin. Solid State Mater. Sci. **10**, 83 (2006).
[2] C. M. Wang, V. Shutthanandan, S. Thevuthasan, T. Doubay, and S. A. Chambers, J. Appl. Phys. **97**, 073502 (2005).
[3] N. H. Hong, J. Sakai, W. Prellier, and A. Hassini, Appl. Phys. Lett. **83**, 3129 (2003).
[4] T. Ohsawa, Y. Matsumoto, and H. Koinuma, Appl. Surf. Sci. **223**, 84 (2004).
[5] L. Sangaletti, M. C. Mozzati, P. Galinetto, C. B. Azzoni, A. Speghini, M. Bettinelli, and C. Calestani, J. Phys.: Condens. Matter **18**, 7643 (2006).
[6] N. H. Hong, J. Sakai, N. Poirot, and V. Brizé, Phys. Rev. B **73**, 132404 (2006).
[7] J. M. Coey, M. Venkatesan, and C. B. Fitzgerald, Nat. Mater. **4**, 173 (2005).
[8] S. Das Sarma, E. H. Hwang, and A. Kaminski, Phys. Rev. B **67**, 155201 (2003); A. Kaminski and S. Das Sarma, Phys. Rev. Lett. **88**, 247202 (2002).
[9] G. Mallia and N. M. Harrison, Phys. Rev. B **75**, 165201 (2007); Jun Chen, Paul Rulis, Lizhi Ouyang, S. Satpathy, and W. Y. Ching, *ibid.* **74**, 235207 (2006); L. A. Errico, M. Renteria, and M. Weissmann, *ibid.* **72**, 184425 (2005).
[10] A. E. Bocquet, T. Mizokawa, T. Saitoh, H. Namatame, and A. Fujimori, Phys. Rev. B **46**, 3771 (1992).
[11] J. W. Quilty, A. Shibata, J.-Y. Son, K. Takubo, T. Mizokawa, H. Toyosaki, T. Fukumura, and M. Kawasaki, Phys. Rev. Lett. **96**, 027202 (2006).
[12] F. Parmigiani and L. Sangaletti, J. Electron Spectrosc. Relat. Phenom. **98-99**, 287 (1999).
[13] T. Droubay, K. M. Rosso, S. M. Heald, D. E. McCready, C. M. Wang, and S. A. Chambers, Phys. Rev. B **75**, 104412 (2007).
[14] V. R. Galakhov, A. I. Poteryaev, E. Z. Kurmaev, V. I. Anisimov, S. Bartkowski, M. Neumann, Z. W. Lu, B. M. Klein, and T. R. Zhao, Phys. Rev. B **56**, 4584 (1997).
[15] Robert D. Cowan, *The Theory of Atomic Structure and Spectra* (University of California, Berkeley, 1981).
[16] J. Zaanen, C. Westra, and G. A. Sawatzky, Phys. Rev. B **33**, 8060 (1986).
[17] P. S. Bagus, R. Broer, W. A. de Jong, W. C. Nieuwpoort, F. Parmigiani, and L. Sangaletti, Phys. Rev. Lett. **84**, 2259 (2000).
[18] T. Uozumi, K. Okada, A. Kotani, R. Zimmermann, P. Steiner, S. Hüfner, Y. Tezuka, and S. Shin, J. Electron Spectrosc. Relat. Phenom., **83**, 9 (1997); R. Zimmermann, P. Steiner, R. Claessen, F. Reinert, and S. Hüfner, *ibid.*, **96**, 179 (1998).
[19] U. Diebold, Surf. Sci. Rep. **48**, 53 (2003).
[20] R. J. Cole, N. J. Brooks, and P. Weightman, Phys. Rev. Lett. **78**, 3777 (1997).
[21] J. Zaanen, G. A. Sawatzky, and J. W. Allen, Phys. Rev. Lett. **55**, 418 (1985).
[22] J. M. D. Coey, Lect. Notes Phys. **678**, 185 (2005).